Journal Pre-proof

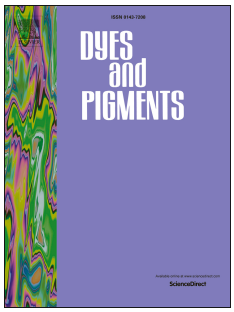

New cationic heptamethinecyanine-graphene hybrid materials

Kyriakos C. Prousis, Ruben Canton-Vitoria, Georgia Pagona, Maria Goulielmaki, Vassilis Zoumpourlis, Nikos Tagmatarchis, Theodora Calogeropoulou

PII: S0143-7208(19)32318-6

DOI: https://doi.org/10.1016/j.dyepig.2019.108047

Reference: DYPI 108047

To appear in: *Dyes and Pigments*

Received Date: 30 September 2019

Revised Date: 6 November 2019

Accepted Date: 12 November 2019

Please cite this article as: Prousis KC, Canton-Vitoria R, Pagona G, Goulielmaki M, Zoumpourlis V, Tagmatarchis N, Calogeropoulou T, New cationic heptamethinecyanine-graphene hybrid materials, *Dyes and Pigments* (2019), doi: https://doi.org/10.1016/j.dyepig.2019.108047.

This is a PDF file of an article that has undergone enhancements after acceptance, such as the addition of a cover page and metadata, and formatting for readability, but it is not yet the definitive version of record. This version will undergo additional copyediting, typesetting and review before it is published in its final form, but we are providing this version to give early visibility of the article. Please note that, during the production process, errors may be discovered which could affect the content, and all legal disclaimers that apply to the journal pertain.

© 2019 Published by Elsevier Ltd.

Journal Pre-proof

New cationic heptamethinecyanine-graphene hybrid materials

Kyriakos C. Prousis,[a, #] Ruben Canton-Vitoria,[b, #] Georgia Pagona,[b] Maria Goulielmaki,[a] Vassilis Zoumpourlis,[a] Nikos Tagmatarchis[b*] and Theodora Calogeropoulou [a*]

[a] Institute of Chemical Biology, National Hellenic Research Foundation, 48 Vassileos Constantinou Avenue, Athens 11635, Greece

[b] Theoretical and Physical Chemistry Institute, National Hellenic Research Foundation, 48 Vassileos Constantinou Avenue, Athens 11635, Greece

[#] Equally contributed.

*Corresponding authors

1. Introduction

Near-infrared (NIR) fluorophores that absorb and emit within the 700–900 nm region have attracted considerable attention by the scientific community due to their diverse applications in biomedical materials and related fields. These dyes have been applied widely as active ingredients in semiconducting and laser materials, optical recording media, paints, and bio probes[[1]]. More specifically, NIR fluorescent dyes have emerged as promising modalities for monitoring the levels of various biologically relevant species in cells and organisms[2,3]. The advantages of NIR probes include minimal interfering absorption and fluorescence from biological samples, inexpensive laser diode excitation, reduced scattering and enhanced tissue penetration depth [[3]]. However, there are only relatively few classes of NIR dyes that are readily available. These include phthalocyanines, cyanines, squaraines and more recently sulfone-rhodamines [5]. In particular, cyanine dyes encompass a large and diverse class of molecules with two aromatic nitrogen-containing heterocycles connected by a polymethine linker. They exhibit large extinction coefficient and high quantum yield values and possess highly tunable structures. The monomethine and trimethinecyanines (Cy3) generally show absorption in the visible region while, heptamethinecyanines (Cy7) may show absorption beyond 1000 nm. In particular, the NIR dye Indocyanine Green (ICG) has been approved by the FDA and has been

Journal Pre-proof

implemented in clinical use [6]. Currently, there is an increasing demand for photostable NIR dyes presenting large Stokes shifts, due to the emerging interest in optical *in vivo* imaging as well as for their applications in the modification of nanomaterials [7].

Graphene is a single graphite plane in which the sp^2 hybridized carbon atoms form a hexagonal lattice. Graphene can be considered as a `building block' for graphite, nanotubes and other carbon materials. Recent progress has shown that graphene-based materials can have a profound impact on electronic and optoelectronic devices, chemical sensors, nanocomposites and energy storage [8-10]. Furthermore, during the past few years, graphene has attracted considerable attention for potential applications in biosensing, biomedical diagnosis and therapy and biotechnological applications due to its unique physical properties and high surface-to-volume ratio allowing the introduction of numerous species upon functionalization [11,12]. Thus, graphene has been functionalized with avidin–biotin, peptides, NAs, proteins, aptamers, small molecules, bacteria, and cells through physical adsorption or chemical conjugation. The functionalized graphene biosystems have been used to generate biological platforms, biosensors, and biodevices [13,14]. Photothermal therapy (PTT) has been pursued during recent years as an alternative cancer therapeutic strategy which relies on the capability of NIR-photoabsorbers to produce heat upon NIR laser irradiation, which in turn results in the thermal ablation of malignant cells. PTT advantages include specificity, minimal invasiveness and spatial-temporal selectivity [15]. The ability of graphene to absorb in the NIR region has prompted its application in the photothermal therapy of cancer. Thus, a variety of functional compounds have been used to decorate graphene aiming to increase the efficiency of the nanocomposites towards cancer therapy and/or imaging modalities [16-20].

In the current study we have synthesized four new near-infrared fluorescent indolenine-based cationic heptamethinecyanine dyes, which were further covalently conjugated to exfoliated graphene. The rationale for the synthesis of the graphene-based hybrid materials is their potential application as an

Journal Pre-proof

optical imaging modality characterised by high cell viability with respect to the cyanine dyes counterparts. Additionally, future applications could involve their application as a delivery platform for high loading efficiency of additional components for theranostic applications.

Specifically, the conjugation of two of the dyes was accomplished via a condensation reaction on pre-modified graphene, while the other two heptamethinecyanines were directly anchored onto exfoliated graphene sheets via the methodology of *in-situ* generated aryl diazonium salt addition. The optical properties of the dyes and the respective graphene-based hybrids were studied using absorbance and fluorescence spectroscopy. In order to get an insight on the potential for biomedical applications two cell lines with distinct characteristics regarding their physiologic state were employed. Thus, a representative of a cancer cell line (RKO), and an undifferentiated, very sensitive non-cancerous progenitor cell line (WJ-MSC human umbilical cord mesenchymal stem cells) were used to evaluate the *in vitro* cytotoxicity and the cell penetrating capacity of the new hybrids and corresponding NIR dyes. The current work goes beyond the state-of-the-art as previous efforts were focused only on the assessment of charge-transfer interactions developed within modified graphene with anionic tricyanofuran-based heptamethinecyanine dyes, formed either through covalent derivatisation [21] or supramolecular functionalisation [22].

2. Experimental section

2.1. Materials and instrumentation

All reactions were carried out under scrupulously dry conditions. THF was distilled over sodium in the presence of benzophenone, DCM was distilled over calcium hydride. ^{1}H NMR spectra were recorded at 600 or 300 MHz, ^{13}C NMR spectra at 150.9 or 75.5 MHz and were internally referenced to residual solvent signals. Data for ^{1}H NMR are reported as follows: chemical shift (δ ppm), multiplicity (s = singlet, br s = broad singlet, d = doublet, dt = doublet of triplets, dd = doublet of doublet, t = triplet, m = multiplet), coupling constant and integration. Data for ^{13}C NMR are reported in terms of chemical shift

(δ ppm). HR-mass spectra were recorded on a UHPLC LC-MS^n Orbitrap Velos-Thermo instrument. Thin Layer Chromatography (TLC) was carried out on precoated silica gel (0.2 mm, 60 F254) glass plates. Chromatographic purification was performed using silica gel (200–400 mesh). Microwave reactions were run on a CEM instrument. Steady-state UV-Vis electronic absorption spectra were recorded on a Perkin Elmer (Lambda 19) UV-Vis-NIR spectrophotometer. Steady-state emission spectra were recorded on a Fluorolog-3 JobinYvon-Spex spectrofluorometer (model GL3-21). Pico-second time-resolved fluorescence spectra were measured by the time-correlated-single-photon-counting (TCSPC) method on a Nano-Log spectrofluorometer (Horiba JobinYvon), by using a laser diode as an excitation source (NanoLED, 654 and 784 nm) and a UV-Vis detector TBX-PMT series (250-850 nm) by Horiba JobinYvon. Lifetimes were evaluated with the DAS6 Fluorescence-Decay Analysis Software. Mid-infrared spectra in the region 500−4500 cm^{-1} were obtained on a Fourier transform IR spectrometer (Equinox 55 from Bruker Optics) equipped with a single reflection diamond ATR accessory (DuraSamp1IR II by SensIR Technologies). Typically, 100 scans were acquired at 2 cm^{-1} resolution. Micro-Raman scattering measurements were performed at room temperature in the backscattering geometry using a RENISHAW inVia Raman microscope equipped with a CCD camera and a Leica microscope. A 2400 lines mm^{-1} grating was used for all measurements, providing a spectral resolution of ± 1 cm^{-1}. As an excitation source the Ar^+ laser (633 nm with less than 2.65 mW laser power) was used. Measurements were taken with 45 seconds of exposure times at varying numbers of accumulations. The laser spot was focused on the sample surface using a long working distance 50x objective. Raman spectra were collected on numerous spots on the sample and recorded with Peltier cooled CCD camera. The intensity ratio I_D/I_G was obtained by taking the peak intensities following any baseline corrections. The data were collected and analyzed with Renishaw Wire and Origin software. Thermogravimetric analysis was performed using a TGA Q500 V20.2 Build 27 instrument by TA in a nitrogen (purity >99.999%) inert atmosphere. Scanning electron

Journal Pre-proof

microscope (SEM) imaging and energy dispersive X-ray spectroscopy (EDS) were performed using a FE-SEM (model JSM-7610F) equipped with an EDAX (X-ACT, Oxford instrument).

2.2 Synthetic procedures

*2.2.1 Synthesis of (3E)-2-chloro-2-(hydroxymethylene)cyclohex-1-enecarbaldehyde (**2**).*

To a solution of dimethylformamide (20 mL, 273 mmol) in 20 mL CH_2Cl_2 at 0 ^oC, a solution of $POCl_3$ (17.5 mL, 115 mmol) in 20 mL CH_2Cl_2 was added dropwise. After 30 min, cyclohexanone was added (5 g, 50 mmol), the resulting mixture was refluxed with vigorous stirring for 3 h at 80 °C, was poured into ice-cold water, and was let it stand overnight to obtain **2** as a yellow solid (7.6 g, 85%) after filtration and drying. ^{1}H NMR (300 MHz, DMSO-d_6) δ: 1.54 – 1.52 (m, 2H), 2.35 (m, 4H), 7.52 (s, 1H), 10.08 (s, 1H), 10.82 (s, 1H). ESI *m/z* $[M+H]^+$ 173.1.

*2.2.2. Synthesis of 1,2,3,3-tetramethyl-3H-indolium iodide (**3**).*

A mixture of 2,3,3-trimethyl-3*H*-indole (2.0 g, 12.6 mmol) and methyl iodide (4.71 mL, 75.3 mmol) in acetonitrile (7.8 mL) was heated at reflux, using microwave irradiation for 15 minutes (130W) (open vessel). The reaction mixture was cooled to room temperature and the solvent evaporated under reduced pressure. The residue obtained was triturated with diethyl ether (20 mL) and the solid was recrystallized from methanol-diethyl ether. The pale yellow crystalline product was filtered, washed with diethyl ether and dried under vacuo over P_2O_5. Yield 3.42 g, 91%. ^{1}H NMR (300 MHz, DMSO-d_6) δ: 1.53 (s, 6H), 2.77 (s, 3H), 3.97 (s, 3H), 7.64 – 7.62 (m, 2H), 7.82 – 7.84 (m, 1H), 7.90 – 7.92 (m, 1H).

*2.2.3. Synthesis of 2-(2-[2-chloro-3-([1,3-dihydro-1,3,3-trimethyl-2H-indol-2-ylidene]ethylidene)-1-cyclohexen-1-yl]ethenyl)-1,3,3-trimethylindolium iodide (**4**)*

1,2,3,3-Tetramethyl-3*H*-indolium iodide (**3)** (2.5 g, 8.31 mmol), dialdehyde **2** (0.478 g, 2.77 mmol) and CH_3COONa (1.36 g, 16.62 mmol) were added to a mixture of acetic acid and acetic anhydride (1:1, 108 mL) and the mixture was heated for 4 h at 120 °C. Subsequently, the solvent was evaporated and the residue was partitioned between CH_2Cl_2 (50.0 mL) and water (30 mL) and the organic layer was dried

over sodium sulphate and the solvent was evaporated *in vacuo*. The crude product was purified by flash column chromatography to yield compound **4** as a green solid (2.84 g, 74%), [eluting solvent system: CH_2Cl_2/CH_3OH, (98:2 to 95:5)]. ^{1}H NMR (300 MHz, DMSO-d_6) δ: 1.67 (s, 12H), 1.92 – 1.79 (dt, J = 11.8, 6.3 Hz, 2H), 2.71 (t, J = 6.0 Hz, 4H), 3.68 (s, 6H), 6.30 (d, J = 14.2 Hz, 2H), 7.25 – 7.33 (m, 2H), 7.44 (d, J = 4.1 Hz, 4H), 7.62 (d, J = 7.3 Hz, 2H), 8.25 (d, J = 14.2 Hz, 2H). ^{13}C NMR (600 MHz, DMSO-d_6) δ: 20.4, 25.9, 27.3, 31.6, 48.8, 101.8, 111.4, 122.3, 125.1, 126.0, 128.5, 140.9, 142.6, 142.8, 147.6, 172.6.

*2.2.4. Synthesis of 6-aminohexanoic acid (**5**)*

6-Bromohexanoic acid (1.0 g, 51.3 mmol) was dissolved in 25% aqueous NH_4OH (40 mL) and the solution was stirred for 24 hours at ambient temperature. The reaction mixture was then evaporated under reduced pressure to give the desired product **5** as a white solid (7.26 g, 99% yield). ^{1}H NMR (300 MHz, CD_3OD) δ: 1.32 – 1.45 (m, 2H), 1.54 – 1.70 (m, 4H), 2.20 (t, J = 6.7 Hz, 2H), 2.87 (t, J = 7.0 Hz, 2H), 3.28 (s, 2H).

*2.2.5. Synthesis of NIR-dye **7***

Compound **4** (25.0 mg, 0.05 mmol), 6-aminohexanoic acid (**5**) (38.5 mg, 0.33 mmol) and triethylamine (109 µL, 0.82 mmol) were dissolved in CH_3OH (2.0 mL) and refluxed at 70 ^{o}C for 4 h. The solvent was evaporated under reduced pressure and the residue was purified by flash column chromatography (95:4:1 CH_2Cl_2/CH_3OH/CH_3COOH) to yield NIR-dye **7** as a blue solid (30 mg, 52%); ^{1}H NMR (300 MHz, CD_3OD) δ: 1.44 – 1.51 (m, 2H), 1.65 (s, 12H), 1.58 – 1.69 (m, 2H), 1.77 – 1.89 (m, 4H), 2.25 (t, J = 7.2 Hz, 2H), 2.56 (t, J = 6.3 Hz, 4H), 3.44 (s, 6H), 3.78 (t, J = 6.8 Hz, 2H), 5.78 (d, J = 13.1 Hz, 2H), 7.05 – 7.11 (m, 4H), 7.29 – 7.38 (m, 4H), 7.77 (d, J = 12.9 Hz, 2H). ^{13}C NMR (150 MHz, CD_3OD) δ: 171.1, 168.9, 145.0, 141.2, 140.2, 129.4, 123.9, 123.0, 121.7, 109.8, 95.6, 51.5, 35.0, 32.2, 29.1, 27.5, 26.0, 25.8, 22.9. ESI-MS: m/z 578.31 $[M]^+$; ESI-MS: m/z 578.39 $[M]^+$. HR-MS (ESI+): $[M]^+$ $C_{38}H_{48}N_3O_2$ calculated for 578.3741, found 578.3737.

*2.2.6. Synthesis of NIR-dye **8***

Compound **4** (50 mg, 0.082 mmol) and thioglycolic acid (9 µL, 0.1 mmol) were dissolved in acetonitrile (10 mL), and one drop of triethylamine was added. The reaction mixture was stirred at room temperature for 15 min, and then the solvent was evaporated. The crude product was purified by flash column chromatography to give NIR-dye **8** (18.7 mg, 70%) as green solid. [eluting solvent system: CH_2Cl_2/CH_3OH, (98:2 to 80:20)]. ^{1}H NMR (300 MHz, CD_3OD) δ: 1.74 (s, 12H), 1.86 – 1.90 (m, 2H), 2.56 (t, *J* = 6.1 Hz, 4H), 3.58 (s, 2H), 3.62 (s, 6H), 5.97 (d, *J* = 14.1 Hz, 2H), 7.05 (d, *J* = 8.1 Hz, 2H), 7.20 (t, *J* = 7.4 Hz, 4H), 7.33 – 7.36 (m, 4H), 9.12 (d, , *J* = 14.1 Hz, 2H). ^{13}C NMR (150 MHz, CD_3OD) δ: 175.1, 174.5, 159.1, 147.5, 144.4, 142.8, 142.5, 134.4, 129.7, 126.0, 123.3, 111.6, 102.1, 50.4, 43.6, 31.6, 28.3, 27.1, 22.7; ESI-MS: m/z 539.29 $[M]^+$. HR-MS (ESI+): $[M]^+$ $C_{34}H_{39}N_2O_2S$ calculated for 539.2727, found 539.2724.

*2.2.7. Synthesis of 4-(2-aminoethyl)benzenamine (**10**)*

To a solution of 2-(4-nitrophenyl)ethanamine hydrochloride (**9**) (1 g, 4.94 mmol) in methanol (25 mL) was added ammonium formate (1.56 g, 24.7 mmol) followed by 10% palladium on carbon (130 mg), and the reaction mixture was refluxed for 24 h. The reaction mixture was filtered through Celite and washed with methanol. The filtrate and washings were combined and the solvent was then evaporated. The crude product was purified by flash column chromatography (CH_2Cl_2/CH_3OH: 80:20) to give 4-(2-aminoethyl)benzenamine hydrochloride salt as a brown solid. The hydrochloride salt was then treated with aqueous NaOH 5N (15 mL), extracted with dichloromethane, dried over Na_2SO_4 and concentrated under reduced pressure to give 4-(2-aminoethyl)benzenamine **10** as brown sticky foam. Yield 0.51 g, 80%. ^{1}H NMR (300 MHz, $CDCl_3$) δ: 2.84 (t, *J* = 6.8 Hz, 2H), 2.90 (t, *J* = 6.9 Hz, 2H), 3.57 (br s, 2H), 6.64 (d, *J* = 8.4Hz, 2H), 6.99 (d, *J* = 8.4Hz, 2H).

*2.2.8. Synthesis of NIR-dye **11***

Compound **4** (50 mg, 0.082 mmol) and 4-(2-aminoethyl)benzenamine (**10**) (21.8 mg, 0.164 mmol) were dissolved in acetonitrile (5 mL). The reaction mixture was heated at reflux for 2h and then stirred

at room temperature for 12h (consumption of starting material was monitored by ESI-MS). Subsequently the solvent was evaporated and the residue was purified by column chromatography (CH_2Cl_2/CH_3OH: 98:2 to 95:5) to give NIR-dye **11** (35 mg, 61%) as green solid. ^{1}H NMR (600 MHz, $CDCl_3$) *δ*: 1.57 – 1.68 (m, 14H), 2.39 (t, *J* = 6.2 Hz, 4H), 3.17 (t, *J* = 6.7 Hz, 2H), 3.34/3.57 (br 2s, 6H), 4.10 (dd, *J* = 5.9, 12.0 Hz, 2H), 5.48 (d, *J* = 9.5 Hz, 2H), 6.58 (d, *J* = 8.1 Hz, 2H), 7.02 – 7.04 (m, 4H), 7.23 – 7.26 (m, 4H), 7.61 (br s, 2H). ^{13}C NMR (300 MHz, CD_3OD) *δ*: 21.3, 25.2, 29.0, 29.7, 36.2, 50.7, 93.9, 108.0, 115.4, 122.1, 122.6, 128.1, 129.8, 137.3, 140.8, 169.7, 172.6; ESI-MS: m/z 583.40 $[M]^+$. HR-MS (ESI+): $[M]^+$ calculated for $C_{40}H_{47}N_4$ 583.3795, found 583.3792.

*2.2.9. Synthesis of tert-butyl 4-(2-hydroxyethyl)phenylcarbamate (**13**)*

To a solution of 2-(4-aminophenyl) ethanol (**12**) (1 g, 7.28 mmol) in ethyl acetate (10 mL) was added di-tert-butyl dicarbonate (1.75 g, 8.02 mmol), and the reaction mixture was stirred for 24 hours at room temperature. Subsequently, water and ethyl acetate were added to the reaction mixture. The organic layer was dried over anhydrous magnesium sulphate and the solvent was removed under reduced pressure. The residue was purified by crystallization with ethyl acetate and petroleum ether to give tert-butyl 4-(2-hydroxyethyl)phenylcarbamate (**13**) (1.64 mg, 95%) as white solid. ^{1}H NMR (300 MHz, $CDCl_3$) *δ*: 1.52 (s, 9H), 2.81 (t, *J* = 6.6 Hz, 2H), 3.82 (br s, 2H), 6.45 (br s, 1H), 7.16 (d, *J* = 8.4 Hz, 2H), 7.29 (d, *J* = 8.4 Hz, 2H).

*2.2.10. Synthesis of dye **16***

Diethyl azodicarboxylate (0.63 mL, 4 mmol) was added to an efficiently stirred solution of triphenyl phosphine (1.50 g, 4 mmol) in 10 mL of freshly distilled tetrahydrofuran at 0 °C. The mixture was stirred at 0 °C for 30 min. A solution of tert-butyl 4-(2-hydroxyethyl)phenylcarbamate (**13**) (0.475 g, 2 mmol) and thioacetic acid (0.28 mL, 4 mmol) in 5 mL tetrahydrofuran was added dropwise over 10 min, and the mixture was stirred for 1 h at 0 °C and 1 h at ambient temperature and a clear yellowish solution was

formed. The reaction mixture was concentrated and the crude product was purified by flash column chromatography (petroleum ether /ethyl acetate: 90:10) to afford thioacetate **14** (0.53, 90% yield)**.**

To a suspension of lithium aluminum hydride (0.37 g, 9.75 mmol) in 2.5 mL of anhydrous tetrahydrofuran was added dropwise a solution of thioacetate **14** (0.53 g, 1.8 mmol) in 4 mL of anhydrous tetrahydrofuran and the reaction mixture was stirred at room temperature for 30 min. The reaction was quenched by the dropwise addition of a solution 95:5 tetrahydrofuran / water (5 mL), then diluted with ethyl acetate (20 mL), dried over sodium sulphate and the solid was filtered through a short celite pad and washed with ethyl acetate (80 mL). The filtrate was evaporated in vacuo to afford tert-butyl 4-(2-mercaptoethyl)phenylcarbamate (**15**) as an oil, which was used directly without any further purification.

Compound **4** (100 mg, 0.164 mmol) and tert-butyl 4-(2-mercaptoethyl)phenylcarbamate (101 mg, 0.4 mmol) were dissolved in acetonitrile (100 mL), and triethylamine (0.5 mL) was added. The reaction mixture was stirred at room temperature for 12 h (consumption of starting material was monitored by ESI-MS), and the solvent was evaporated. The crude product was purified by flash column chromatography to give dye **16** (85 mg, 64 %) as green solid. [eluting solvent system: CH_2Cl_2/CH_3OH, (98:2 to 95:5)]. ^{1}H NMR (600 MHz, CD_3OD) δ: 1.50 (s, 9H), 1.66 (s, 12H), 1.89 – 1.93 (m, 2H), 2.66 (t, J = 5.8 Hz, 4H), 2.92 (t, J = 6.9 Hz, 2H), 3.09 (t, J = 6.9 Hz, 2H), 3.63 (s, 6H), 6.24 (d, J = 14.2 Hz, 2H), 7.10 (d, J = 8.4 Hz, 2H), 7.25 (t, J = 7.4 Hz, 2H), 7.29 (d, J = 7.9 Hz, 2H), 7.33 (d, J = 8.2 Hz, 2H), 7.41 (t, J = 7.3 Hz, 2H), 7.50 (d, J = 7.3 Hz, 2H), 8.82 (d, J = 14.2 Hz, 2H). ^{13}C NMR (300 MHz, CD_3OD) δ: 22.3, 27.1, 28.2, 28.7, 31.6, 36.4, 40.4, 50.3, 80.8, 102.0, 111.7, 120.1, 123.4, 126.1, 129.8, 130.0, 134.5, 135.0, 139.3, 142.4, 144.4, 147.2, 155.3, 158.5, 174.5. ESI-MS: m/z 700.30 $[M]^+$. HR-MS (ESI+): $[M]^+$ calculated for $C_{45}H_{54}N_3O_2S$ 700.3931, found 700.3931.

*2.2.11. Synthesis of NIR-dye **17***

Compound **16** (42 mg, 0.073 mmol) was dissolved in a solution of trifluoroacetic acid and dichloromethane (9:1, 2 mL) and stirred for 1 h at room temperature. The solvents were evaporated and the residue was recrystallized with methanol/diethyl ether to give NIR-dye **17** (45 mg, 75%) as green solid. ^{1}H NMR (300 MHz, CD_3OD) δ: 1.65 (s, 12H), 1.80 – 1.85 (m, 2H), 2.65 (br s, 4H), 2.72 (br s, 2H), 2.96 (br s, 2H), 3.65 (s, 6H), 6.27 (d, J = 14.1 Hz, 2H), 6.51 (br s, 2H), 6.84 (br s, 2H), 7.26 (t, J = 6.6 Hz, 2H), 7.37 – 7.44 (m, 4H), 7.59 (d, J = 7.0 Hz, 2H), 8.71 (d, J = 14.1 Hz, 2H). ^{13}C NMR (300 MHz, CD_3OD) δ: 22.3, 27.2, 28.2, 31.6, 36.9, 40.1, 50.3, 102.1, 111.7, 120.8, 123.3, 126.2, 129.8, 130.8, 134.6, 136.7, 138.3, 142.3, 144.4, 147.1, 158.4, 174.5. ^{19}F NMR (300 MHz, CD_3OD) δ: -76.9. The trifluoroacetic salt of **17** was transformed to the free amino compound **17** by treatment with triethylamine . ESI-MS: m/z 600.39 $[M]^+$. HR-MS (ESI+): $[M]^+$ $C_{40}H_{46}N_3S$ calculated for 600.3407, found 600.3407.

2.3 Preparation of graphene-based hybrid materials

*2.3.1 Synthesis of hybrid materials **21** and **22**.*

In a typical reaction, 15 mg of derivatized exfoliated graphene **20** [24,25] were dispersed by sonication in 10 mL of dry dichloromethane under nitrogen atmosphere. Then, the cyanine dye (15 mg, 0.021 mmol for **7** and 10 mg, 0.015 mmol for **8**) was added, followed by the quick addition of 4-dimethylaminopyridine (8.2 mg, 0.067 mmol) and 1-ethyl-3-(3-dimethylaminopropyl) carbodiimide (5.5 mg, 0.035 mmol), and stirred at reflux for 96 hours. After that period, the reaction mixture was cooled down to room temperature, filtered over a PTFE membrane filter (pore size 0.1 μm) and washed with a large amount of dichloromethane to remove completely any organic residual matter. The newly prepared graphene-based hybrid materials **21** and **22** were obtained as solids and stored under dark.

*2.3.2. Synthesis of hybrid materials **23** and **24**.*

In a typical reaction, 10 mg of exfoliated graphene were dispersed by sonication in 10 mL of 1,2-dichlorobenzene, under a nitrogen atmosphere. Then, a solution of the NIR dye (30 mg, 0.042 mmol for

Journal Pre-proof

aniline derivative cyanine dye **11** and 35 mg, 0.049 mmol for aniline derivative cyanine dye **17**) in 5 mL of acetonitrile was added, followed by the quick addition of isoamyl nitrite (10 mg, 0.085 mmol) and the reaction mixture was stirred at 60 ^{o}C, under N_2, for 96 hours. After cooling down to room temperature, the reaction mixture was diluted with 30 mL of dimethylformamide, filtered over a PTFE membrane filter (pore size 0.1 μm) and washed with a large amount of dimethylformamide and CH_2Cl_2 to remove completely any organic residuals. The newly prepared graphene-based hybrid materials **23** and **24** were obtained as solids and stored under dark.

2.4. In vitro cytotoxicity

2.4.1 Cell lines

RKO human colon adenocarcinoma cell line was obtained from American Type Culture Collection (ATCC). Cells were grown in 75-cm^2 flasks (Corning) in D-MEM medium supplemented with 10% foetal bovine serum (FBS), antibiotics and amino acids (all from Invitrogen). Wharton's Jelly Mesenchymal Stem Cells (WJ-MSC) were isolated from donated Umbilical Cord tissue samples from normal, full-term deliveries following approval by the institutional bioethics review board. Isolation and culture protocols followed for WJ-MSC are fully described in Christodoulou *et al*., 2013 [23]. Briefly, cells were cultured in 75-cm^2 flasks (Corning), in DMEM/F12 (with 3.5 g/L glucose, ultraglutamine I, and Na pyruvate; Lonza) supplemented with 10% batch-tested FBS, 15 mM 2-[4-(2-hydroxyethyl)piperazin-1-yl]ethanesulfonic acid (HEPES), 1x nonessential amino acids, and 1% penicillin/streptomycin (all from Invitrogen). All cells were maintained in a humidified chamber with 5% CO_2 in air at 37 °C with media changes every 3-4 days until 70%–80% confluence.

2.4.2. Cell viability assay

For growth studies the crystal violet (Sigma Aldrich) assay was used. Firstly, cells were seeded into 96-well micro titre plates (Corning) in a density of 4000 cells/well and were allowed to attach overnight (cancer cells) or for 48h (stem cells). The cells were then treated with different concentrations of the

Journal Pre-proof

dyes diluted in DMSO and the correspondent graphene-hybrid material solutions (dH_2O + 0.4% DMSO) for 24 h. Thereafter, cells were fixed with methanol and stained with 0.2% (w/v) crystal violet and the dye was released in 33% (v/v) acetic acid. The absorbance was measured at 595 nm (Tecan, Austria). The cell number in treated versus control wells was estimated and the percentage of viable cells was plotted each time. SD was used for error bar generation. Statistical analysis was performed with one-way ANOVA, post-hoc Bonferroni test in Graphpad Prism 6.0.

2.5. Two-dimensional culture for immunocytochemistry (ICC)

For the ICC 2D culture experiments, cells (10000 cells/well) were grown on coverslips in 24 well plates (Corning) in the appropriate culture medium, at 37 °C for 24 h and then treated with the selected dyes diluted in DMSO and the correspondent graphene-hybrid material solutions (dH_2O + 0.4% DMSO) for 4h. Cells were fixed with 4% paraformaldehyde and washed with PBS (Invitrogen) to remove dead cells. Photographs of the 2D cultures were taken under confocal microscope (Leica 626 TCS SPE confocal laser scanning microscope) after the appropriate staining. LAS AF software was used for image acquisition (Leica Lasertechnik, Heidelberg, Germany). Cell nuclei were stained with Hoechst No. 33342 (Sigma Aldrich, B2261).

3. Results and discussion

3.1. Chemistry

Our initial efforts were focused on the design and synthesis of new NIR dyes, exploiting the tricarbocyanine scaffold as template. Previous studies have shown that compounds of this general structure possess high photostabilities and high polar extinction coefficients [7]. Taking advantage of the facile displacement of the chloro substituent, at the central vinyl carbon of the tricarbocyanine scaffold, by various nucleophiles, appropriate linkers were introduced, which could in turn be covalently ligated to the exfoliated graphene surface either through amide bond formation or via in-situ generated aryl diazonium salt addition [24]. Variation of the heteroatom linkage to the carbocyanine core (Nitrogen or

Sulfur) enabled us to tune the photophysical properties of the synthesised NIR-fluorescent dyes. The synthesis of the new dyes is described in Schemes 2-4 and in Scheme 5 of the corresponding hybrids.

The symmetrical tricarbocyanine core **4**, which was employed as the key common starting material for all the NIR dyes of the present study was prepared as described in Scheme 1. Thus, all (3*E*)-2-chloro-2-(hydroxymethylene)cyclohex-1-enecarbaldehyde (**2**) was prepared via a Vilsmeier–Haack reaction from cyclohexanone (**1**), using phosphorus oxychloride and dimethylformamide in dichloromethane under reflux, followed by condensation with 1,2,3,3- tetramethyl-3*H*-indolium iodide (**3**) to afford compound **4**.

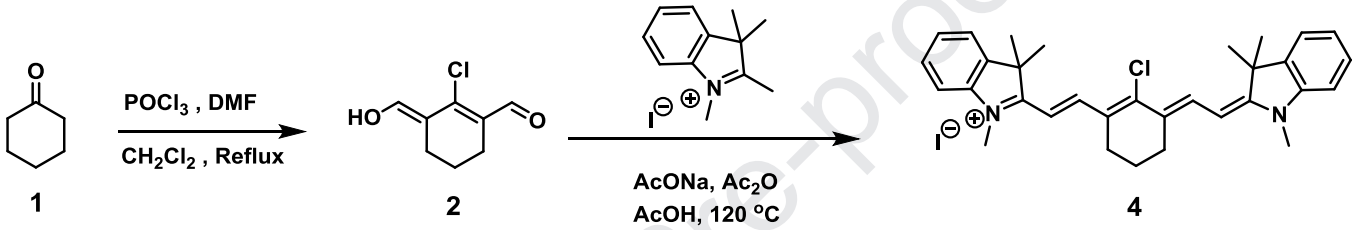

Scheme 1. Synthesis of chloro tricarbocyanine core scaffold **4.**

NIR-fluorescent dyes **7** and **8** bearing a terminal carboxyl group suitable for an amide linkage to the amino-functionalised exfoliated graphene, were prepared from the chloro-tricarbocyanine derivative **4** and 6-aminohexanoic acid or thioacetic acid, respectively (Scheme 2).

Journal Pre-proof

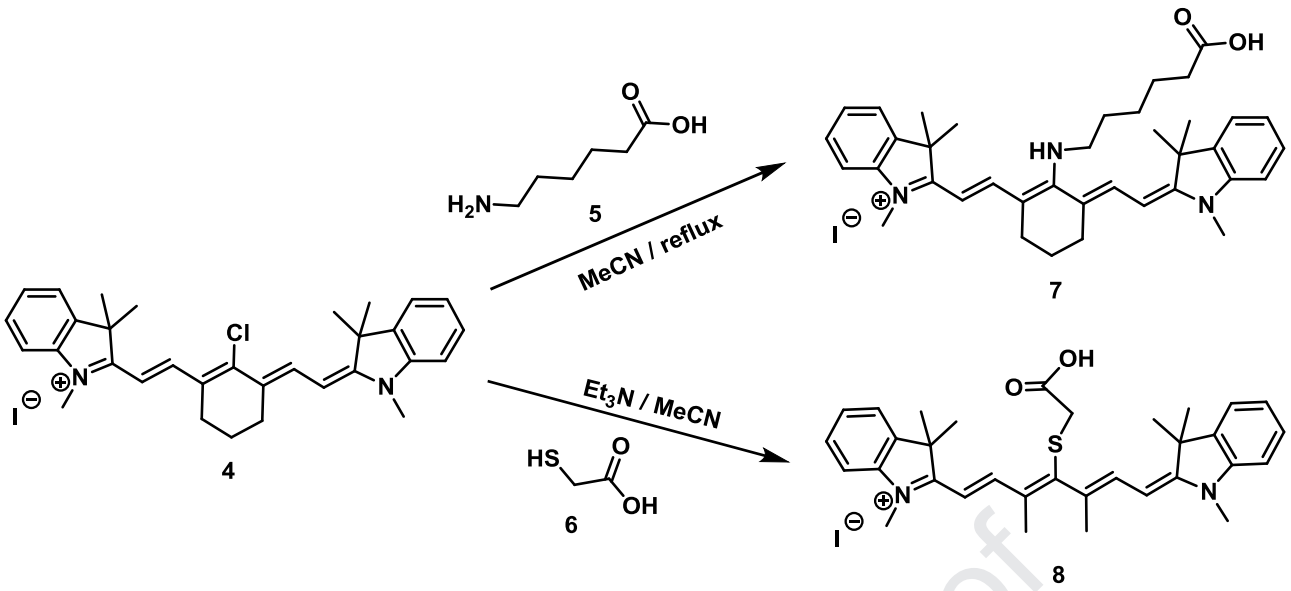

Scheme 2. Synthesis of NIR fluorescent dyes **7** and **8**.

The synthesis of NIR-dyes **11** and **17**, suitable for covalent attachment to exfoliated graphene through the in-situ generated aryl diazonium salt, was effected as described in Schemes 3 and 4, respectively. Thus, reaction of 4-(2-aminoethyl)aniline (**10**), prepared by the catalytic transfer hydrogenation of *p*-nitrophenethylamine hydrochloride (**9**) using palladium on carbon and ammonium formate, with the chloro-tricarbocyanine derivative **4** afforded the desired NIR fluorescent dye **11** (Scheme 3).

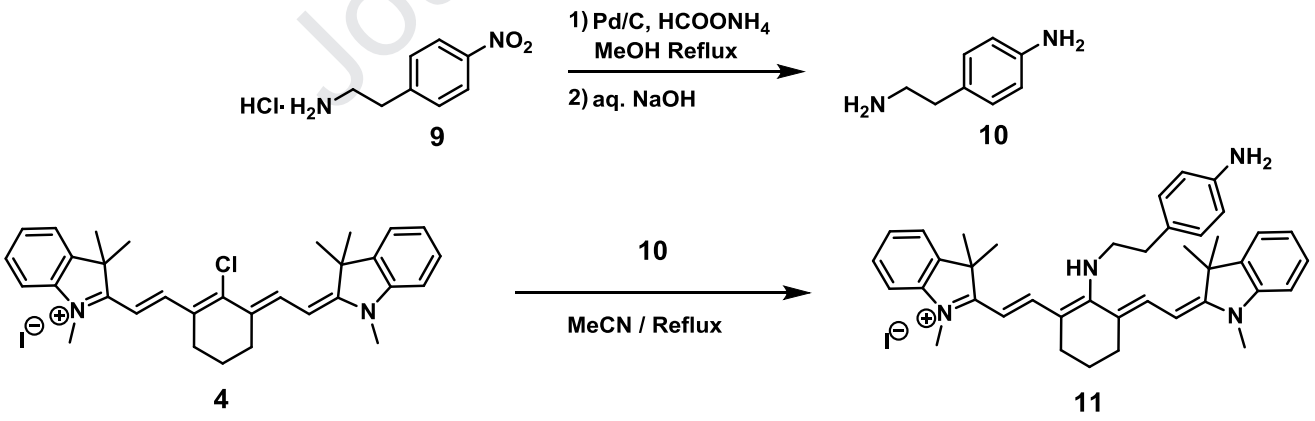

Scheme 3. Synthesis of NIR fluorescent dye **11**.

The thio congener of **11** dye **17**, was prepared as shown in Scheme 4. Protection of the amino group in 2-(4-aminophenyl)ethanol (**12**) using tert-butyloxycarbonyl (BOC) anhydride afforded BOC-protected amino alcohol **13,** which was transformed to the thioacetate ester **14** via Mitsunobu reaction which in turn, was reduced using lithium aluminium hydride to afford thiol **15**. Reaction of thiol **15** with the chloro-tricarbocyanine derivative **4** gave the thio NIR-fluorescent dye **16**. Removal of the BOC protecting group using trifluoroacetic acid in dichloromethane afforded the desired dye **17** bearing a free aniline moiety (Scheme 4).

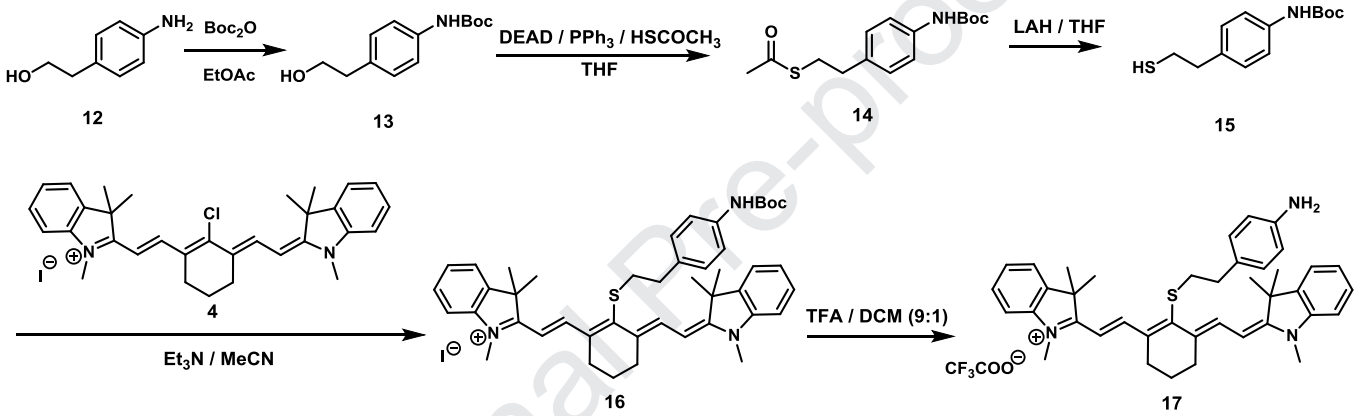

Scheme 4. Synthesis of NIR fluorescent dye **17**.

3.2. Optical properties of NIR dyes 7, 8, 11 and 17

Following the synthesis of the new dyes we studied their optical properties. The fluorescence spectrum ($\lambda_{exc.}$ 620 nm) of carboxy bearing NIR-dye **7** shows an emission band centred at 750 nm, while in the excitation spectrum a band at 620 nm is evident (Supplementary Information, Fig. S1). Conversely, the presence of a thio group in NIR dye **8** results in a red-shift of both the excitation and the emission wavelength compared to the amino–substituted congener, NIR-dye **7**. As shown in Supplementary Information, Fig. S2, in the excitation spectrum of dye **8** a band at 775 nm with a shoulder at 700 nm is evolved, while the corresponding emission band ($\lambda_{exc.}$ 775 nm) is observed at 800 nm. For amino-substituted aniline NIR-dye **11** the excitation and emission ($\lambda_{exc.}$ 650 nm) bands are observed at 657 and

761 nm (Supplementary Information, Fig. S3), respectively. Similar to the case of NIR dye **8**, the excitation and emission ($\lambda_{exc.}$ 720 nm) bands of dye **17** are further red-shifted at 787 and 808 nm (Supplementary Information, Fig. S4), respectively.

3.3. Synthesis of exfoliated graphene-based hybrids 21-24

The preparation of graphene-based hybrid materials **21-24** covalently modified with cyanine dyes **7, 8, 11** and **17,** respectively, is shown in Scheme 5. The main routes to obtain graphene involve either physical processes (mechanical cleavage, epitaxial growth etc) or chemical means (intercalation, oxidation-reduction, surfactants-polymers, functionalization etc), with each method having its own scope and limitations [25].

For the synthesis of hybrids **21** and **22** exfoliated graphene, obtained upon treatment of graphene with chlorosulfonic acid according to a previously reported procedure [26], was functionalized through a diazotization reaction [27]. employing *N*-BOC protected aniline derivative **18** and isoamyl nitrite to *in-situ* form the aryl diazonium salt capable to covalently add to the graphene skeleton. Cleavage of the BOC protecting group by trifluoroacetic acid resulted to a plethora of amino groups onto the graphene sheets that were further reacted with the carboxylic acid group of cyanine dyes **7** and **8**, following activation using *N*-(3-dimethylaminopropyl)-*N'*-ethylcarbodiimide hydrochloride (EDCI), yielding hybrids **21** and **22**, respectively.

In turn, hybrids **23** and **24** were prepared from exfoliated graphene [26], and the aryl diazonium salts of cyanine dyes **11** and **17** formed *in situ* upon treatment with isoamyl nitrite.

Journal Pre-proof

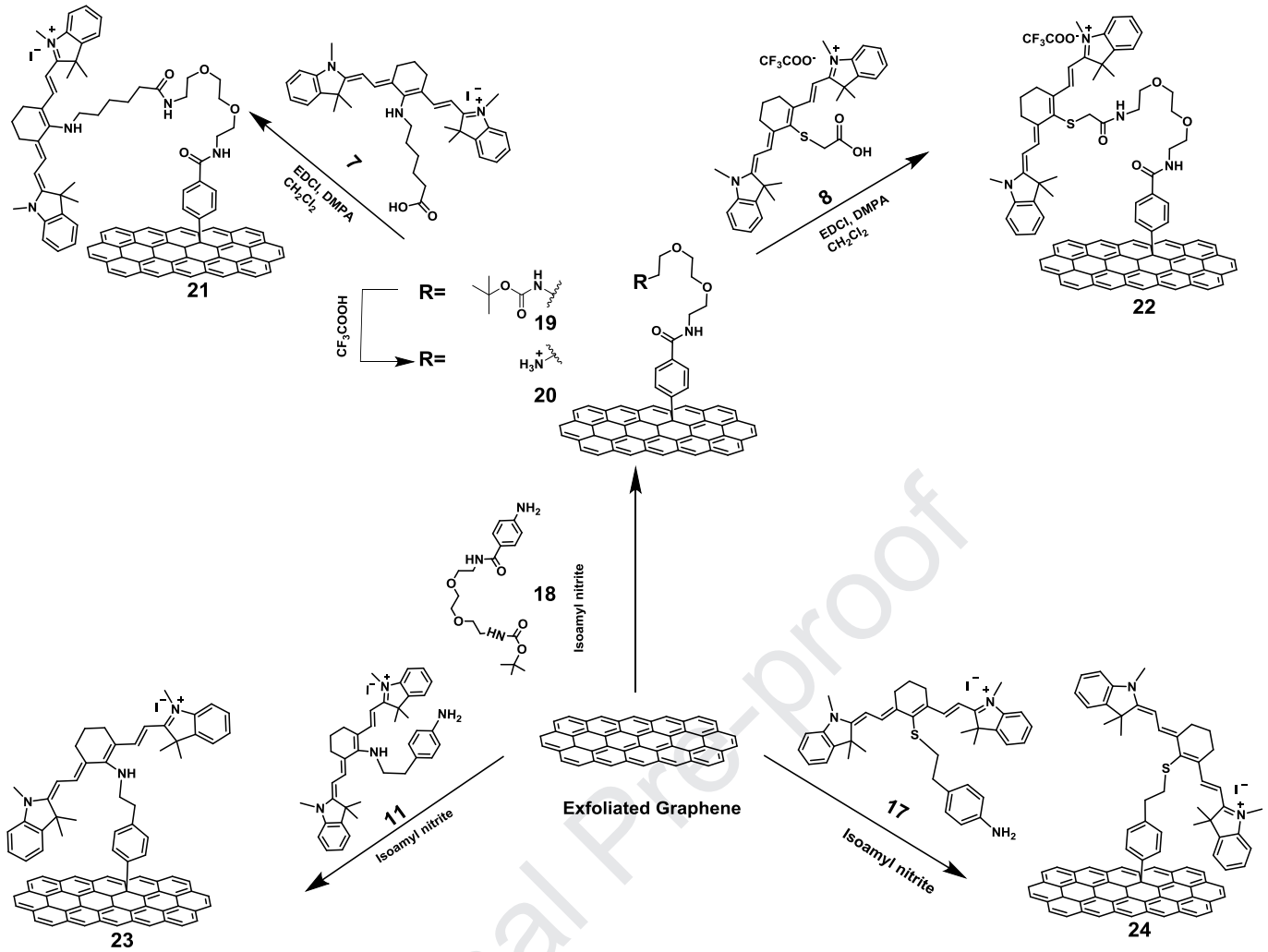

Scheme 5. Preparation of graphene-based hybrid materials **21-24**.

3.4. Characterisation of exfoliated graphene-based hybrids 21-24

The characterization of hybrid materials **21-24** was accomplished by complementary spectroscopic, thermal and microscopy imaging means.

Initially, Raman spectroscopy was employed to corroborate the successful covalent modification of exfoliated graphene with the *in-situ* formed aryl diazonium salt, resulting in material **19** which was further utilised for the preparation of hybrids **21** and **22**. In the Raman spectrum of **19**, three bands located at 1330, 1580 and 2670 cm^{-1} are discernible as shown in Figure 1. The G-band at 1580 cm^{-1} is attributed to vibrations due to sp^2 hybridized carbon atoms, while the D-band at 1330 cm^{-1} is ascribed to vibrations due to defect sites and sp^3 hybridized carbon atoms. The shape and frequency of the 2D band

located at 2670 cm^{-1} is sensitive to the number of graphene sheets [28,29]. Evidently, an increased D/G ratio is found for **19** as compared with that owed to exfoliated graphene (I_D/I_G = 0.42 for **19**; I_D/I_G = 0.20 for exfoliated graphene), highlighting the success of the covalent functionalization reaction on graphene sheets. Furthermore, the D/G ratio for materials **21** and **22** was found unaltered (I_D/I_G = 0.42) as compared to that of **19**, in accordance with the fact that the cleavage of the BOC unit followed by condensation with cyanine dyes **7** and **8**, respectively, does not disrupt further the graphene skeleton. In addition, the G-band for hybrids **21** and **22** was marginally shifted by ca. 3 cm^{-1}, as compared to the value registered for exfoliated graphene, implying the development of charge-transfer phenomena between the NIR dyes and the graphene sheets. The 2D band for hybrids **21** and **22** is deconvoluted and fitted with four and one Lorentzians, respectively (Supplementary Information, Fig. S5). The full-width-half-maximum value for the 2D band of **21** and **22** was calculated to be 82 and 79 cm^{-1}, respectively, thereby, accordingly indicating the presence of monolayered and bilayered graphene sheets [28,30,31]. Notably, the first indication for the successful preparation of **21** and **22** arose by employing the Kaiser test (c.f. Supplementary Information). The latter enabled us to quantify the amount of free amine groups in **21** and **22**, ca. 15 μmol g^{-1}, which was found significantly lower as compared with the one found in the precursor modified graphene **20**, ca. 140 μmol g^{-1}, hence proving the success of the condensation reaction between **20** and cyanines **7** and **8**. Furthermore, the work up procedure followed for the isolation of all hybrids including **21** and **22** ensures the absence of any physisorbed dye **7** and **8** onto graphene. More specifically, the work up procedure involves filtration over PTFE membrane filter with pore size 100 nm, to remove organic materials and impurities, followed by extensive washing with dichloromethane, a solvent that dissolves the dyes **7** and **8**, until examination of the filtrate shows no absorbance due to dyes.

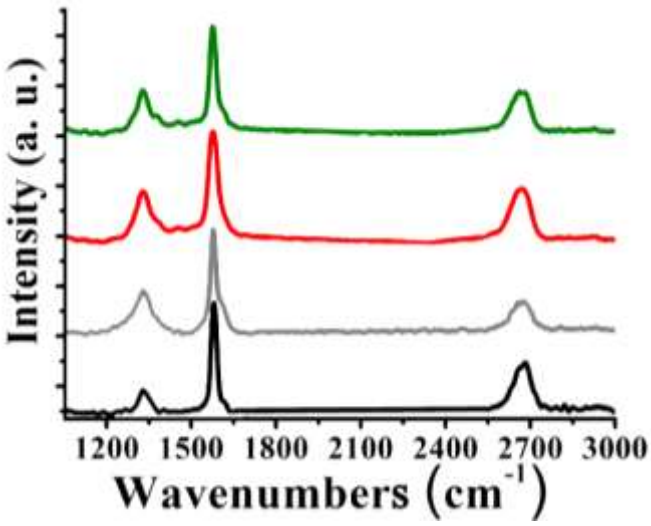

Figure 1. Raman spectra for exfoliated graphene (black) and graphene-based materials **19** (grey), **21** (green), and **22** (red), normalized at the G-band and obtained upon 633 nm excitation.

The covalent bonding of cyanines dyes **11** and **17** on exfoliated graphene yielding hybrid materials **23** and **24**, respectively, is corroborated based on Raman spectroscopic studies. More specifically, in the Raman spectra of **23** and **24**, the evolvement of the characteristic D-band, which is due to the presence of sp^3 hybridized carbon atoms, in both hybrids was evidenced. In turn, this band is absent in the Raman spectrum of exfoliated graphene (Supplementary Information, Fig. S6).

Subsequently, attenuated-total-reflectance infra-red (ATR-IR) studies further confirmed the effective coupling of dyes **7** and **8** onto exfoliated graphene. In graphene-based material **19**, characteristic strong carbonyl vibrations at 1698 and 1630 cm^{-1} attributed to the presence of benzamide and BOC units, respectively, were evident. Markedly, in **20** the latter was absent, reflecting the effective cleavage of BOC group that gives rise to the presence of free $–NH_2$ groups. In graphene-based hybrid material **21**, the carbonyl amide vibration was found enhanced as a result of the formation of new amide band at 1640 cm^{1}, while the vibration at 1720 cm^{-1} owed to the carboxylic acid moiety of the free cyanine dye **7** had accordingly disappeared (Figure 2). Similar observations can be made for the ATR-IR spectrum of

hybrid **22** (Supplementary Information, Fig. S7). In the ATR-IR spectra of dyads **23** and **24** only the C-H stretching vibration modes were discernible at 2800-2900 cm^{-1} (Supplementary Information, Fig. S8).

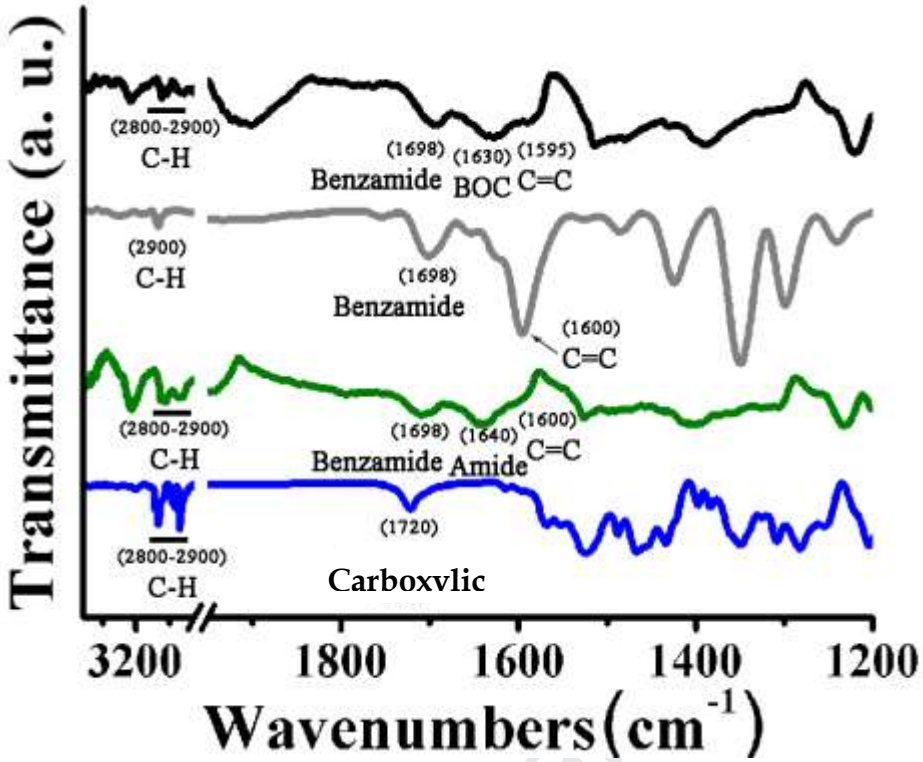

Figure 2. ATR-IR spectra for graphene-based materials **19** (black), **20** (grey), **21** (green) and cyanine dye **7** (blue).

The degree of graphene functionalization for **21** and **22** was evaluated by thermogravimetric analysis (TGA). Graphene is thermally stable at high temperatures under inert atmosphere and this is shown in the corresponding TGA graph (Figure 3, black line). Covalently functionalized graphene-based materials possess characteristic TGA graphs since organic addends thermally decompose in a temperature range of 200-550 ºC, while beyond that temperature the thermal decomposition of the graphene skeleton at sites with sp^3 hybridized carbon atoms takes place. This explains the continuous mass loss observed in the TGA graphs for functionalized graphene-based materials **21-24**. For modified graphene-based material **20**, a mass loss of 12% was observed in the temperature range 200-560 °C, while for hybrids **21**

and **22** the corresponding mass loss was 22 % and 17 %, respectively (Figure 3). On this basis, the loading of cyanine dyes **7** and **8** onto graphene was calculated as 1 per every 270 and 360 carbon atoms for **21** and **22**, respectively. Analogously, from the thermal decomposition of **23** and **24** and the mass loss observed, 2 % and 8 %, respectively, the loading of **11** and **17** was calculated to be 1 unit per every 1560 and 900 carbon atoms for **23** and **24**, respectively (Supplementary Information, Fig. S9). Although this represents a rather small amount of dyes incorporated onto the graphene sheets, it is consistent with the small perturbation of graphene lattice in **23** and **24** upon the covalent incorporation of **11** and **17**, as revealed with the small enhancement of the D-band in the corresponding Raman spectra (cf. Supplementary information, Fig. S6).

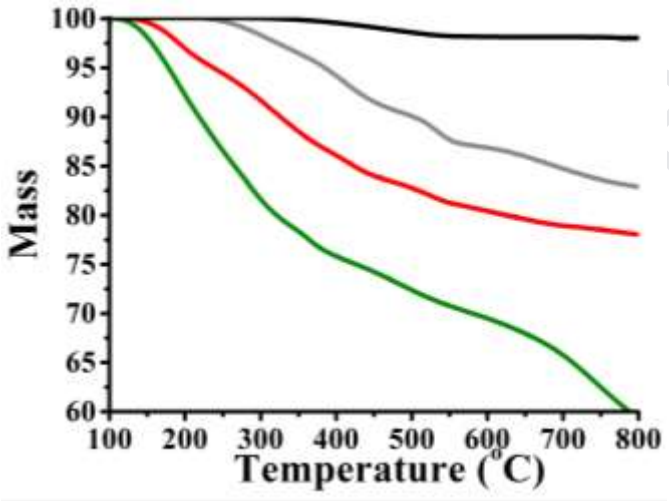

Figure 3. TGA graphs for exfoliated graphene (black), graphene-based material **20** (grey), and hybrids **21** (green) and **22** (red), obtained under nitrogen atmosphere.

The morphology of graphene-based hybrid materials **21-24** was examined by FE-SEM imaging. Briefly, after dispersing the material by mild sonication in hexane, a drop was deposited onto the sample holder and examined. A representative image for **21**, shown in Figure 4, reveals the presence of overlapping oligolayered graphene sheets, of various sizes, with typical folding and ripple patterns. Although the exact number of layers cannot be accurately estimated, the absence of large graphitic particles is

obvious, as it is also proven by Raman spectroscopy (*cf*. Figure 1). Similar were the morphological findings for the hybrids **22**, **23** and **24** (Supplementary Information, Fig. S10). The SEM image of exfoliated graphene (Supplementary Information, Fig. S11) is very similar to the images obtained for hybrids **21-24**, which further supports that **21-24** are based on graphene sheets.

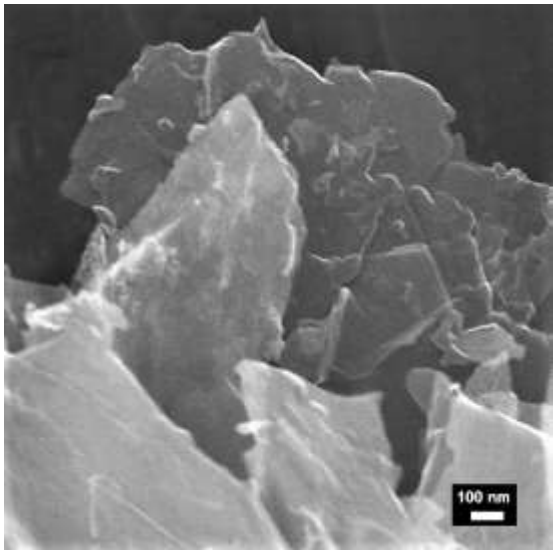

Figure 4. Representative FE-SEM image for graphene-based hybrid **21**.

The dispersibility of hybrids **21**-**24** was enhanced in polar solvents such as DMF, allowing to perform spectroscopic studies in solution. Hence, examining possible ground-state interactions between cyanine dyes **7** and **8** with graphene within hybrid materials **21** and **22**, respectively, UV-Vis-NIR studies were performed. The electron absorption spectrum for **21** obtained in DMF, showed the characteristic continuous absorption in the NIR region owed to graphene, followed by a broadened band centred at 660 nm (Figure 5a), corresponding to free cyanine dye **7** possibly possessing different conformational structures on graphene. This finding not only guarantees the successful integration of **7** onto graphene, by covalently forming hybrid **21**, but also indicates appreciable electronic interactions between the two species at the ground state. In the case of hybrid **22**, the UV-Vis-NIR spectrum is a simple superposition of the absorption spectra owed to graphene and cyanine dye **8** (Figure 5b), suggesting the absence of appreciable interactions in the ground state. The low loading of **11** and **17** within hybrids **23** and **24** (*cf*.

Supplementary Information, Fig. S9), respectively, handicapped the electronic absorption measurements. In the latter, the characteristic absorption bands due to **11** and **17**, centred at 657 and 787 nm, respectively, were masked under the continuous and strong absorbance of graphene (Supplementary Information, Fig. S12).

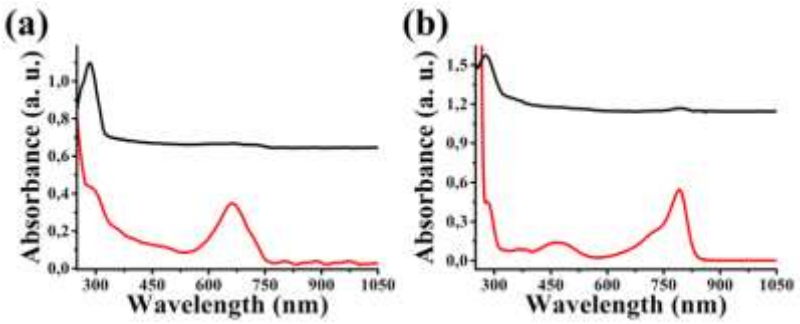

Figure 5. UV-Vis electronic absorption spectra for **(a)** free cyanine dye **7** (red) and graphene-based hybrid material **21** (black), and **(b)** free cyanine dye **8** (red) and graphene-based hybrid material **22** (black), obtained in DMF.

Next, focusing on excited state interactions, photoluminescence assays for hybrids **21** and **22** in comparison with the corresponding free cyanine dyes **7** and **8**, for samples displaying equal absorbance at the excitation wavelength, were performed. Upon 660 nm excitation, **7** revealed a broad emission band centred at 757 nm (Figure 6a). Markedly, in hybrid **21**, the latter emission was found significantly depressed, indicating strong electronic interactions between graphene and **7**, within **21** at the excited state, following electron and/or energy transfer as the decay mechanism of the singlet excited state of ^{1}**7***. Then, on the basis of the time-correlated-single-photon-counting method, the photoluminescence lifetime profiles for **7** were acquired. Analysis of the time-profile of the decay at 757 nm upon excitation at 654 nm for the ^{1}**7*** was monoexponentially fitted with a lifetime of 0.84 ns. On the other hand, the decay component in hybrid **21** was found to be 500 ps. Analogously, the photoluminescence of hybrid **22**, at 810 nm was found quenched as compared to the one attributed to the free cyanine dye **8** (Figure 6b), while the corresponding lifetimes for **8** and **22** were evaluated as 0.81 ns and 250 ps, respectively.

The photoluminescence spectra for hybrids **23** and **24**, as compared with those of the corresponding free cyanine dyes **11** and **17** are presented in the Supplementary Information, Fig. S13. In addition, the emission time profiles for graphene-based hybrids **23** and **24** were characterized by quicker decays, as compared with those registered for the free cyanine dyes **11** and **17**, respectively, and in analogy with those belonging to hybrids **21** and **22**. Collectively, those findings are related with intra-hybrid transduction of electron and/or energy from the electron donors **7, 8, 11** and **17** to graphene in hybrids **21**-**24**, respectively. The emission rate constant (k^S) and quantum yield (Φ^S) for free cyanine dyes **7, 8, 11** and **17** and graphene-based hybrid materials **21**-**24** were calculated based on equations (1) and (2), respectively, and are presented in Table 1.

Equation 1: $k^S = (1/\tau_f)_{\mathbf{hybrid}} - (1/\tau_f)_{\mathbf{dye}}$, where τ_f is the fluorescence lifetime

Equation 2: $\Phi^S = k^S/(1/\tau_f)_{\mathbf{hybrid}}$

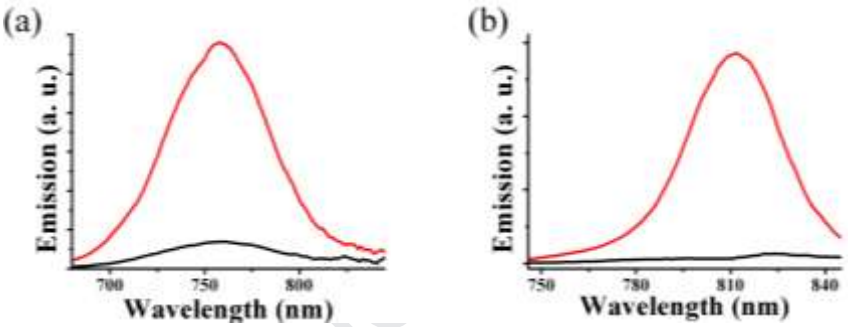

Figure 6. Photoluminescence spectra (excitation at 660 nm) for (a) free cyanine dye **7** (red) as compared with hybrid **21** (black), and (b) free cyanine dye **8** (red) as compared with hybrid **22** (black), obtained in DMF.

Next, shedding light on the redox properties of the hybrid materials, cyclic voltammetry (CV) measurements performed on acetonitrile employing Bu_4NPF_6 as electrolyte in a standard three-electrode cell with glassy carbon as working electrode and platinum wires as counter and pseudoreference electrodes were conducted. Hybrid materials **21** and **22** exhibit a reversible oxidation

at 0.80 and 0.11 V versus Fc/Fc^+, cathodically shifted by approximately 10 and 4 mV, respectively, as compared with the oxidation processes registered for the corresponding free cyanine dyes **7** and **8**. These shifts are attributed to intra-hybrid electronic interactions between the dyes and graphene sheets, rendering easier the oxidation of the latter within the graphene-based hybrid materials. Furthermore, a peak at -0.45 V associated with the reduction of graphene similarly with other reports [9,32], as well as additional reversible reduction processes centred at -1.24 and -1.06 V, were identified in hybrids **21** and **22**. Disappointingly, due to the limited solubility of **23** and **24** we were not able to register suitable and reliable redox data. Collectively, the redox data are presented in Table 1.

Table 1. Photophysical and electrochemical data for cyanine dyes **7, 8, 11** and **17** and graphene-based hybrids **21-24**.

Material	τ_f (ps)	k^S (s^{-1})	Φ^S	$E_{Ox.}$ (V)	$E_{Red.}^1$ (V)	$E_{Red.}^2$ (V)
Cyanine dye **7**	840			0.90		-1.19
Hybrid **21**	500	8.10×10^8	0.40	0.80	-0.45	-1.24
Cyanine dye **8**	810			0.15		-1.16
Hybrid **22**	250	2.77×10^9	0.69	0.11	-0.45	-1.06
Cyanine dye **11**	1183			0.35		-1.34
Hybrid **23**	475	1.26×10^9	0.48	N/A [a]	N/A [a]	
Cyanine dye **17**	1074			0.20		-1.35
Hybrid **24**	366	1.81×10^9	0.67	N/A [a]	N/A [a]	

[a] not registered due to limited solubility

3.5. Cytotoxicity and in vitro imaging studies.

3.5.1 Cell viability study

The biocompatibility of dyes **7**, **8**, **11**, **17** and the corresponding graphene-based hybrid materials **21-24** was examined using the RKO human colon adenocarcinoma cell line and WJ-MSC human umbilical cord mesenchymal stem cells. The crystal violet cell viability assay was used to assess cytotoxicity. The free cyanine dyes **7, 8, 11** and **17** were examined in a range of concentrations (1, 2, 5, 10, and 20 μM). The corresponding hybrids for comparison were tested at the same μg/mL concentrations as the respective dyes. The small differences between the percentages, either above or below 100%, are attributed to statistical errors (Figures 7A and 7B). In general, the graphene-hybrid materials are well-tolerated by both cancer and stem cells, since a reduction in cell viability not higher than 20% was observed only for hybrid **23** for the examined concentration range. Regarding the NIR dyes, the results are diverse for the tested cell lines. NIR dyes **7** and **8** bearing a terminal carboxylic acid functionality are well tolerated by cancer cells showing some toxicity at the high concentration (20 μM). However, there is a difference with respect to stem cells with dye **7** substituted by an aminohexanoic acid moiety, being non toxic, versus dye **8** which possesses a thioacetic acid functionality exhibiting some toxicity at concentrations higher than 2μM. Conversely, dye **17** bearing a para-thioethylaniline moiety exhibits toxicity against RKO and WJ-MSC cells at concentrations higher than 2 μM which is more pronounced against the latter cell line. Finally, dye **11** substituted by a para-aminoethylaniline group is less toxic against stem cells versus cancer cells. Apparently, the presence of the sulfur versus the nitrogen heteroatom increases toxicity in this compound class. In addition, cell morphology was also not affected by the non-toxic concentration treatment, as checked under light microscope (data not shown). These results indicate that the incorporation of the above dyes on graphene renders the resulting hybrid materials more biocompatible and well-tolerated by cultured human cells.

Journal Pre-proof

A **RKO**

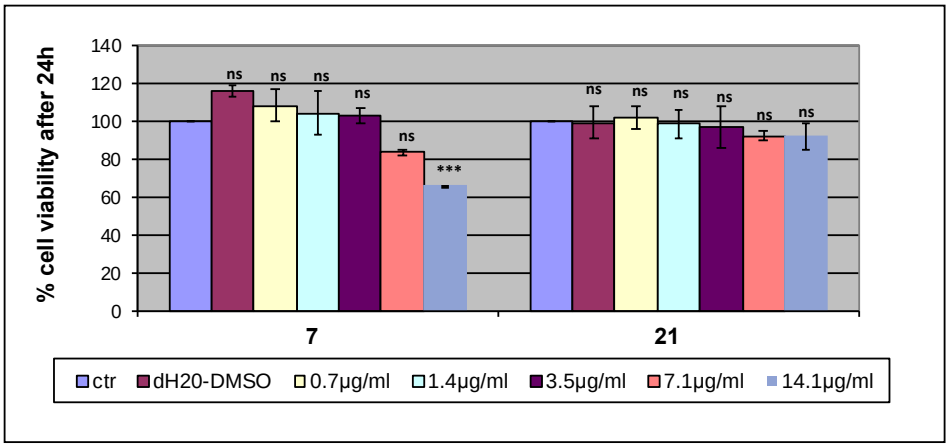
% cell viability after 24h
140
120
100
80
60
40
20
0
ns
ns
ns
ns
ns
***
ns
ns
ns
ns
ns
ns
7
21
ctr
dH20-DMSO
0.7µg/ml
1.4µg/ml
3.5µg/ml
7.1µg/ml
14.1µg/ml

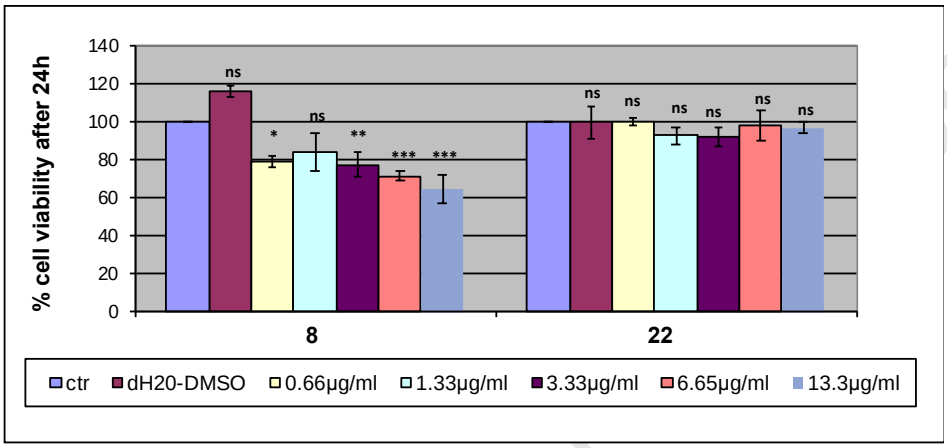
% cell viability after 24h
140
120
100
80
60
40
20
0
ns
*
ns
**
***
***
ns
ns
ns
ns
ns
ns
8
22
ctr
dH20-DMSO
0.66µg/ml
1.33µg/ml
3.33µg/ml
6.65µg/ml
13.3µg/ml

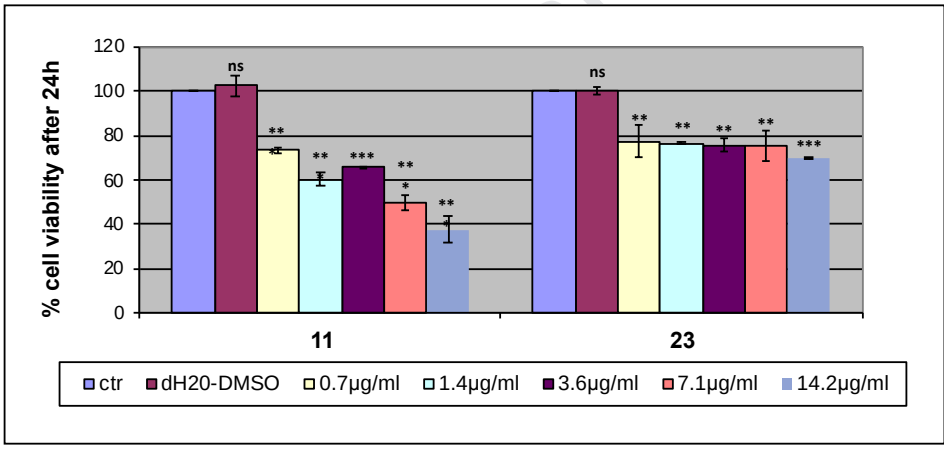
% cell viability after 24h
120
100
80
60
40
20
0
ns
**
**
***
**
*
**
ns
**
**
**
**
***
11
23
ctr
dH20-DMSO
0.7µg/ml
1.4µg/ml
3.6µg/ml
7.1µg/ml
14.2µg/ml

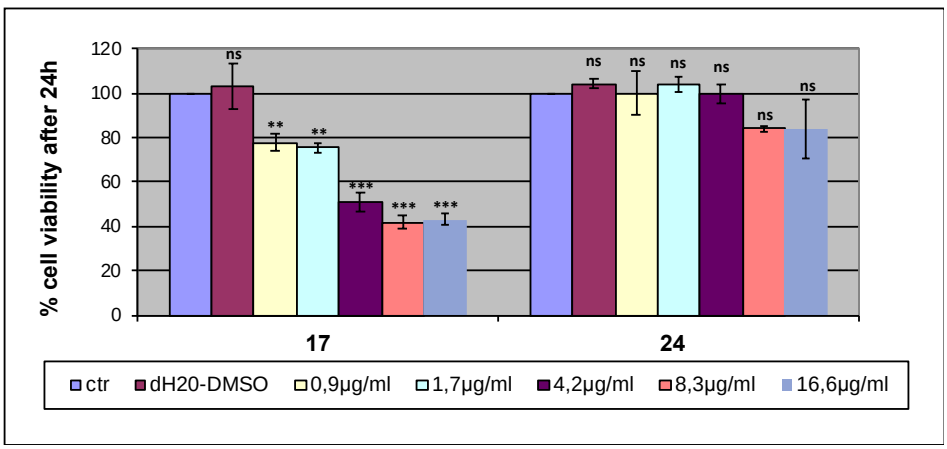
% cell viability after 24h
120
100
80
60
40
20
0
ns
**
**
***
***
***
ns
ns
ns
ns
ns
ns
17
24
ctr
dH20-DMSO
0,9µg/ml
1,7µg/ml
4,2µg/ml
8,3µg/ml
16,6µg/ml

B **WJ-MSC**

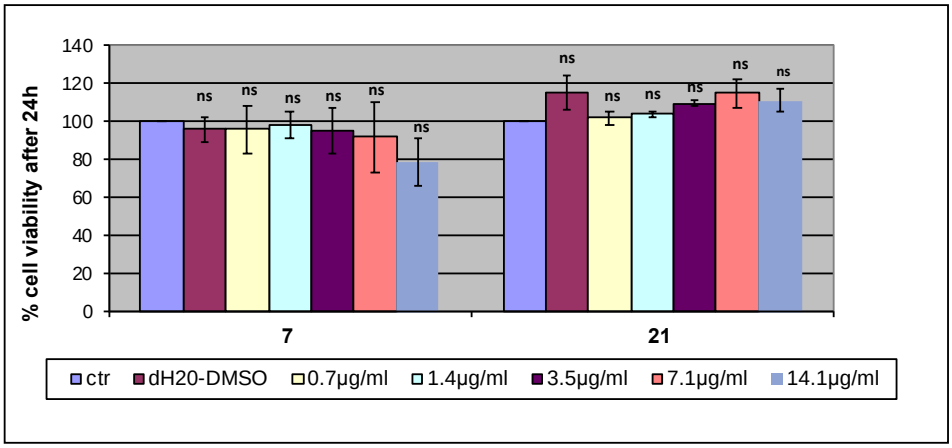
% cell viability after 24h
140
120
100
80
60
40
20
0
ns
7
21
ctr
dH20-DMSO
0.7µg/ml
1.4µg/ml
3.5µg/ml
7.1µg/ml
14.1µg/ml

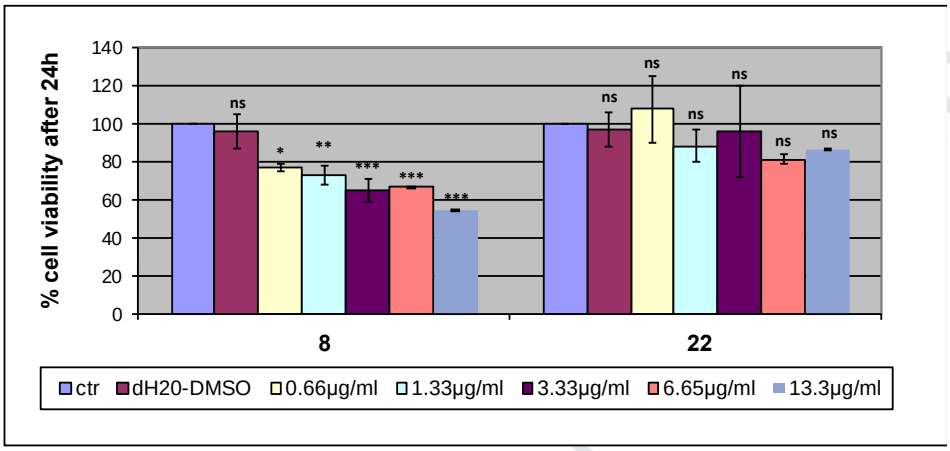
% cell viability after 24h
140
120
100
80
60
40
20
0
ns
*
**
***
8
22
ctr
dH20-DMSO
0.66µg/ml
1.33µg/ml
3.33µg/ml
6.65µg/ml
13.3µg/ml

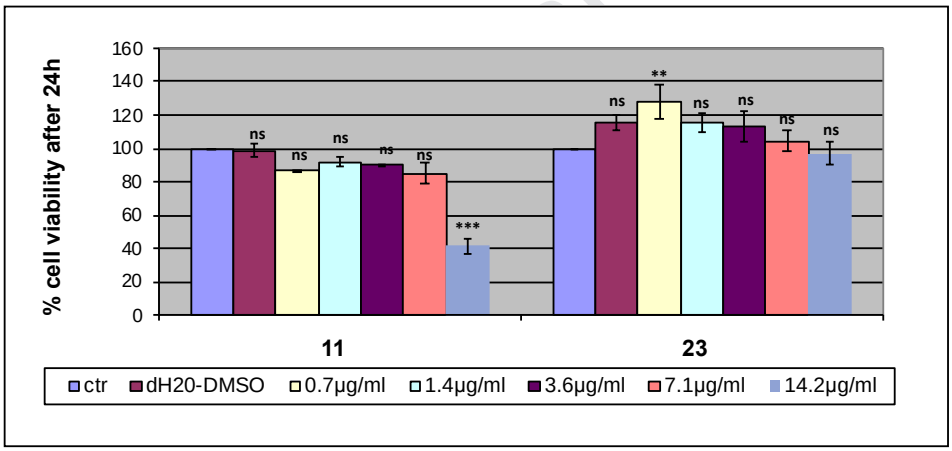
% cell viability after 24h
160
140
120
100
80
60
40
20
0
ns
**
***
11
23
ctr
dH20-DMSO
0.7µg/ml
1.4µg/ml
3.6µg/ml
7.1µg/ml
14.2µg/ml

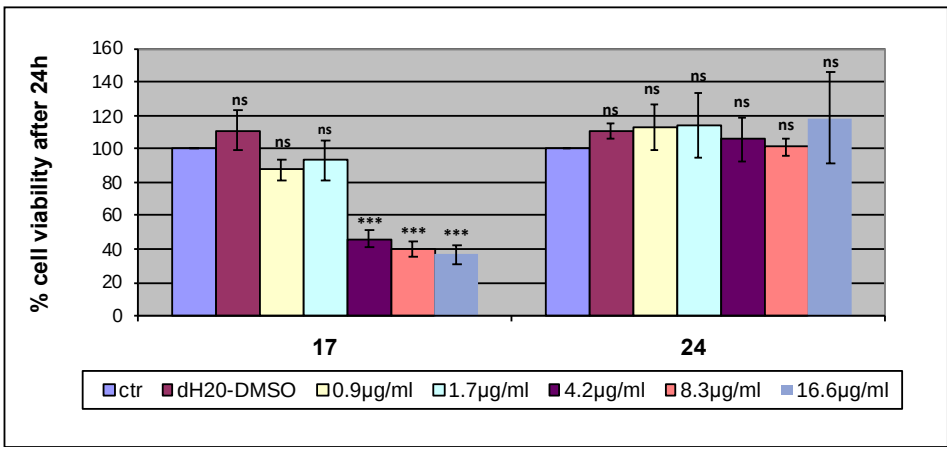
% cell viability after 24h
160
140
120
100
80
60
40
20
0
ns
***
17
24
ctr
dH20-DMSO
0.9µg/ml
1.7µg/ml
4.2µg/ml
8.3µg/ml
16.6µg/ml

Figure 7. Cell viability in **A.** RKO colon cancer cell line and **B.** Wharton's Jelly Mesenchymal Stem Cells (WJ-MSC) after 24h treatment with different concentrations of the four graphene-hybrid materials **21**, **22**, **23**, **24** (right side of each plot) and the respective free cyanine dyes **7, 8, 11, 17** (left side of each plot). The concentrations of the dyes can also be expressed as micromolar (1, 2, 5, 10, 20 μM). As a negative control, cell viability after treatment with the correspondent solvent (DMSO for the dyes, dH_2O+ 0.4% DMSO for the graphene-based hybrids) was measured. Data are representative of two independent experiments, each one performed in duplicates. SD was used for error bar generation. *p<0.05, **p<0.01, ***p<0.001, ns: p>0.05. Statistical significance shown represents the comparison of each sample with the control.

3.5.2. Intracellular imaging

In order to explore their potential application for intracellular imaging and drug delivery protocols, the hybrid materials and the correspondent dyes were observed under confocal fluorescence microscope, after their incubation with RKO or WJ-MS cells for 4 hours. Cell nuclei became visible after DNA staining with Hoechst in order to check whether the above materials are able to enter the cell cytoplasm and in that case to further visualize their dispersion within the cells. All of the examined dyes were able to enter the cells with a high efficacy resulting in intense fluorescence signals which were markedly reduced in the case of the respective graphene-based materials as observed in Figures 8A and 8B. However, stronger signals could be achieved after increasing the tested concentrations, since higher concentrations of the hybrids were not cytotoxic, as discussed above. Pink color stains can be observed in the images of dyes **7**, **8** and **11** in RKO cells, which result from the overlapping of the blue (Hoechst) and red (dyes) staining, and thus could indicate an interaction of the dyes with the nuclear DNA. However, the inability of the other materials to overlap with the nuclear DNA could be attributed to a higher quantity needed in order to achieve this effect. This was not tested, since we opted to employ concentrations that didn't induce cytotoxic effects (*c.f.* Figures 7A and 7B).

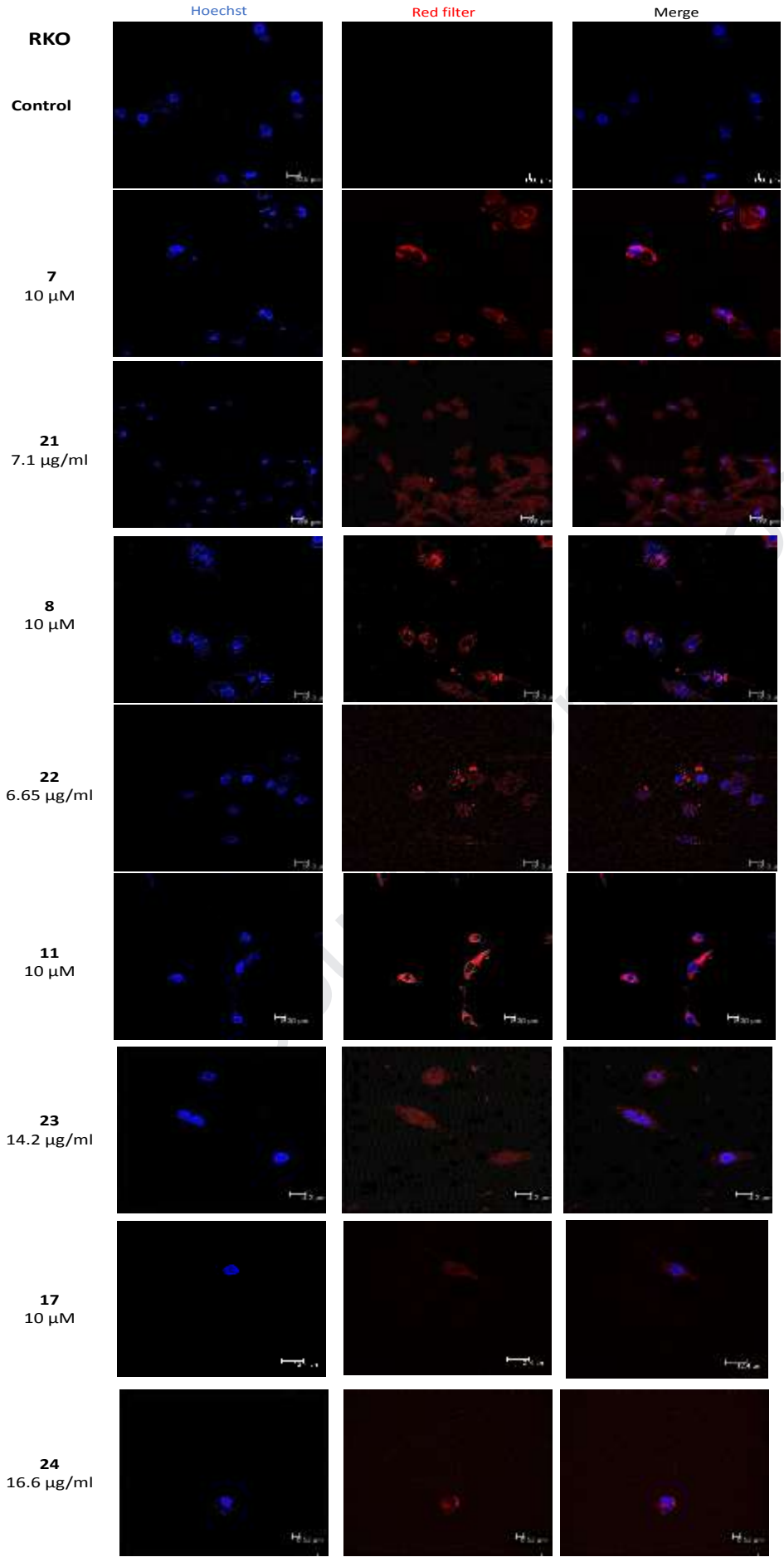
Hoechst
Red filter
Merge
RKO
Control
7
10 µM
21
7.1 µg/ml
8
10 µM
22
6.65 µg/ml
11
10 µM
23
14.2 µg/ml
17
10 µM
24
16.6 µg/ml

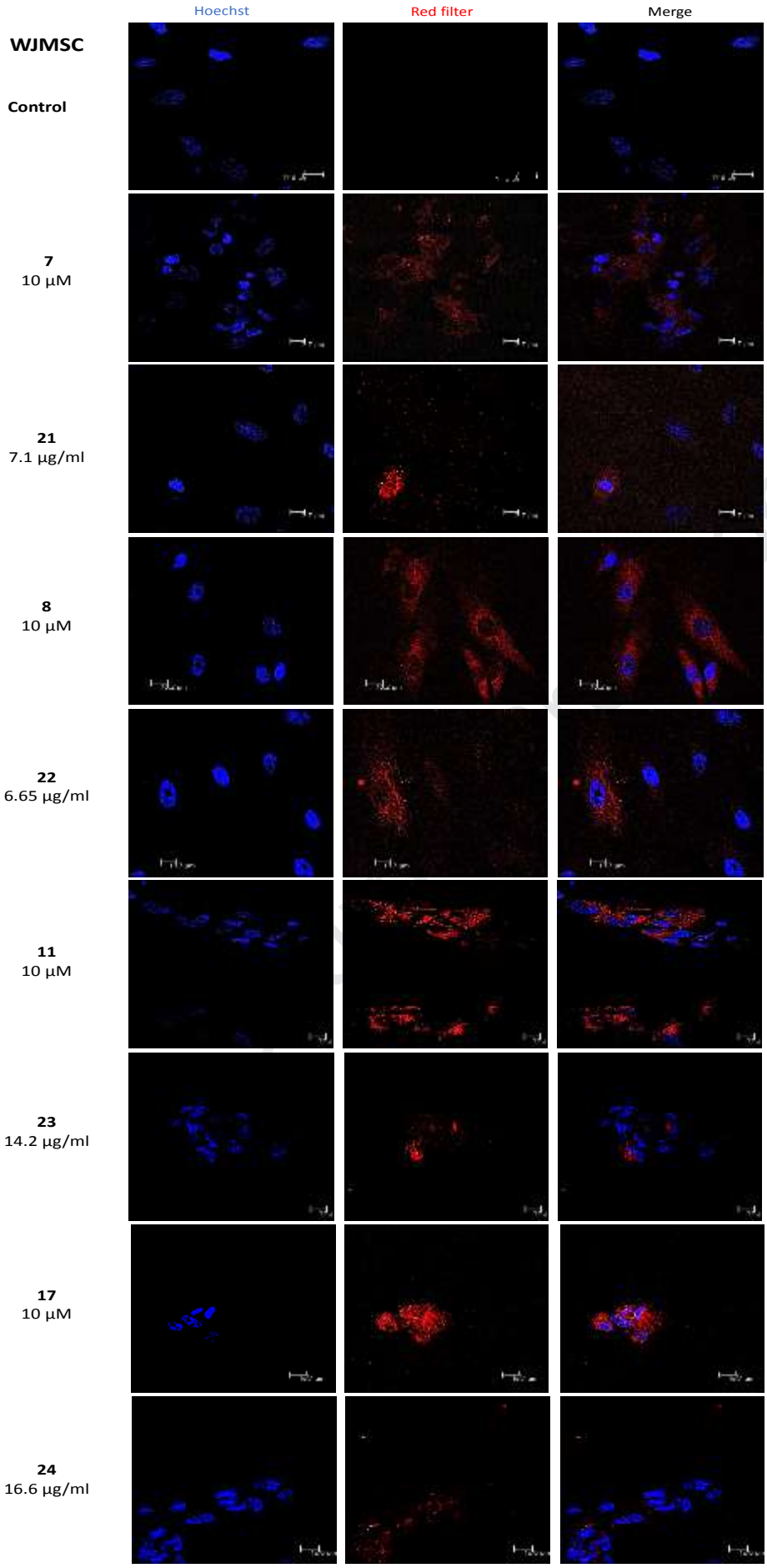
Hoechst
Red filter
Merge
WJMSC
Control
7
10 µM
21
7.1 µg/ml
8
10 µM
22
6.65 µg/ml
11
10 µM
23
14.2 µg/ml
17
10 µM
24
16.6 µg/ml

Figure 8. Images obtained from confocal fluorescence microscope of the four graphene-hybrid materials and the respective dyes in **A.** RKO cell line and **B.** Wharton's Jelly Mesenchymal Stem Cells (WJ-MSC) after incubation for 4h, excited by 361 nm (Hoechst staining) and 581 nm irradiation. Cell nuclei were stained with Hoechst 33342. Magnification x40.

4. Conclusions

In conclusion, we have synthesized NIR indolenine-based cationic heptamethinecyanine fluorescent dyes **7**, **13**, **15**, **17** and their hybrids with exfoliated graphene **21–24.** Cell viability studies using RKO human colon adenocarcinoma cell line and WJ-MSC human umbilical cord mesenchymal stem cells revealed the absense of toxicity of the graphene-based dyads in both cell lines. Cellular uptake studies using confocal microscopy showed that graphene-NIR dyes hybrids are able to enter the cells with high efficacy. Future studies will be focused on assessing the suitablity of the new cyanine-graphene hybrids in bio-applications and in particular for the photothermal therapy of cancer.

Conflicts of interest

The authors declare no conflict of interest.

Acknowledgements

This work was partially funded by the John S. Latsis Public Benefit Foundation. The sole responsibility for its content lies with its authors. In addition, partial funding from the European Union's Horizon 2020 research and innovation programme under the Marie Sklodowska-Curie grant agreement No 642742 is acknowledged. In addition, we acknowledge support of this work by the project "Bioimaging-GR." (MIS 5002755) which is which is funded by the Operational Programme "Competitiveness, Entrepreneurship and Innovation" (NSRF 2014-2020) and co-financed by Greece.

We would like to thank Dr. C. Chochos of the Institute of Chemical Biology / National Hellenic Research Foundation for SEM imaging acquisition. The work of MG was supported by the Hellenic Foundation for

Research and Innovation (HFRI) and the General Secretariat for Research and Technology (GSRT), under the HFRI PhD Fellowship grant (GA. no. 2400).

References

[1] Z. Y. Wang, "Near-Infrared Organic Materials and Emerging Applications" CRC Press **2013.**

[2] Z. Guo, S. Park, J. Yoon, I. Shin, *Chem. Soc. Rev.,* 2014, **43**, 16.

[3] U. B. Lade, P. K. Bhoyar, M. H. Hingankar, *WJPPS*, 2014, **3**, 2193.

[4] J. O. Escobedo, O. Rusin, S. Lim, R. M. Strongin, *Curr. Opin. Chem. Biol*., 2010, **14**, 64.

[5] J. Liu, Y.-Q. Sun, H. Zhang, H. Shi, Y. Shi, W. Guo, *ACS Appl. Mater. Interfaces,* 2016, **8** 22953.

[6] J. T. Alander, I. Kaartinen, A. Laakso, T. Patil, T. Spillmann, V. V. Tuchin, M. Venermo, P. Valisuo, *Int. J. Biomed. Imaging,* 2012, Article ID 940585, 26 pages.

[7] Y.-T. Hang, A. Samanta, M. Vendrell, N.-Y. Kang, K. K. Maiti, K. S. Soh, D. U. K. S. Amma, D. M. Olivo, *WO 2011/119114A1*, 2011.

[8] K. S. Novoselov, V. I. Falko, L. Colombo, P. R. Gellert, M. G. Schwab, K. Kim, *Nature*, 2012, **490**, 192.

[9] N. Karousis, J. Ortiz, A. Sastre-Santos, T. Hasobe, K. Ohkubo, S. Fukuzumi, N. Tagmatarchis, *J. Phys. Chem. C,* 2012, **116**, 20654.

[10] N. Karousis, A. S. D. Sandanayaka, T. Hasobe, S. P. Economopoulos, E. Sarantopoulou, N. Tagmatarchis, *J. Mater. Chem*., 2011, **21**, 109.

[11] H. Zhang, H. Zhang, A. Aldalbahi, X. Zuo, C. Fan, X. Mi, Biosens. *Bioelectron.,* 2017, **89**, 96.

[12] Y. Wang, Z. Li, J. Wang, J. Li, Y. Lin, *Trends Biotechnol.*, 2011, **29**, 205.

[13] G. Shim, M.-G. Kim, J. Y. Park, Y.-K. Oh, *Adv. Drug Deliv. Rev.,* 2016, **105**, 205.

[14] S. Syama, P. V. Mohanan, *Nano-Micro Lett.,* 2019, **11**, 6

[15] V. Shanmugam, S. Selvakumar, C.S. Yeh, *Chem. Soc. Rev.,* 2014, **43**, 6254.

[16] L. Zou, H. Wang, B. He, L. Zeng, T. Tan, H. Cao, X. He, Z. Zhang, S. Guo, Y. Li, *Theranostics,* 2016, **6**, 762.

[17] O. Taratula, M. Patel, C. Schumann, M. A Naleway, A. J. Pang, H. He, O. Taratula, *Inter. J. Nanomedicine,* 2015, **10**, 2347.

[18] Y.-W. Chen, Y.-L. Sub, S.-H. Hu, S.-Y. Chen, *Adv. Drug Deliv. Rev*., 2016, **105**, 190.

[19] L. Cheng, C. Wang, L. Feng, K. Yang, Z. Liu, *Chem. Rev.,* 2014, **114**, 10869.

[20] D. Hu, J. Zhang, G. Gao, Z. Sheng, H. Cui, L. Cai, *Theranostics,* 2016, **6**, 1043.

[21] L. Rodríguez-Pérez, C. Villegas, M. Á. Herranz, J. L. Delgado, N. Martín, *ACS Omega,* 2017, **2**, 9164.

[22] A. Roth, C. Schierl, A. Ferrer-Ruiz, M. Minameyer, L. Rodríguez-Pérez, C. Villegas, M[a] A. Herranz, N. Martín, D. M. Guldi, *Chem,* 2017, **3**, 164.

[23] I. Christodoulou, F. N. Kolisis, D. Papaevangeliou and V. Zoumpourlis, *Stem Cells Int.* 2013, Article ID 246134, 12 pages, doi: 10.1155/2013/246134.

[24] S. P. Economopoulos, G. Rotas, Y. Miyata, H. Shinohara, N. Tagmatarchis, *ACS Nano,* 2010, **4**, 7499.

[25] S. P. Economopoulos, N. Tagmatarchis, *Chem. Eur. J., 2*013, **19**, 12930.

[26] A. Stergiou, H. B. Gobeze, I. D. Petsalakis, S. Zhao, H. Shionhara, F. D'Souza, N. Tagmatarchis, *Nanoscale,* 2015, **7**, 15840.

[27] E. Bekyarova, M. E. Itkis, P. Ramesh, C. Berger, M. Sprinkle, W. A. de Heer, R. C. Haddon, *J. Am. Chem. Soc,.* 2009, **131**, 1336.

[28] A. C. Ferrari, J. C. Meyer, V. Scardaci, C. Casiraghi, M. Lazzeri, F. Mauri, S. Piscanec, D. Jiang, K. S. Novoselov, S. Roth, A. K. Geim, *Phys. Rev. Lett.,* 2006, **97**, 187401.

[29] A. Gupta, G. Chen, P. Joshi, S. Tadigadapa, P. C. Eklund, *Nano Lett*., 2006, **6**, 2667.

[30] Y. Hao, Y. Wang, L. Wang, Z. Ni, Z. Wang, R. Wang, C. K. Koo, Z. Shen, J. T. L. Thong, *Small,* 2010, **6**, 195.

[31] L. M. Malard, M. A. Pimenta, G. Dresselhaus and M. S. Dresselhaus, *Phys. Rep*., 2009, **473**, 51.

[32] A. Stergiou and N. Tagmatarchis, *ACS Appl. Mater. Interfaces,* 2016, ***8*****,** 21576.

Journal Pre-proof

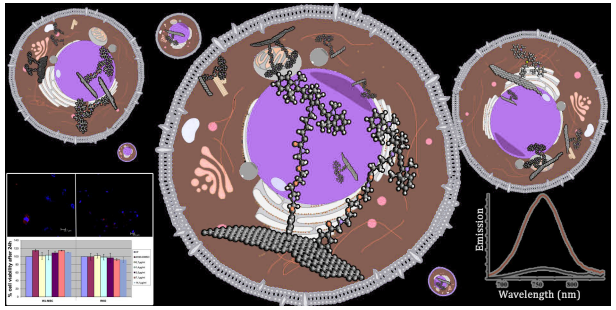

New exfoliated graphene/NIR cationic heptamethinecyanine fluorescent dyes hybrids, able to enter the cells with high efficacy and devoid of toxicity.

Journal Pre-proof

- Four near-infrared fluorescent indolenine-based cationic heptamethinecyanine dyes and their hybrids with exfoliated graphene were prepared.

- The substitution on the tricarbocyanine core and the linkage with exfoliated graphene affects the physicochemical and optical properties.

- Both the NIR-dyes and the graphene-based hybrid materials were able to enter the cells with a high efficacy.

- The graphene-based hybrid materials didn't show toxicity against RKO cancer cell line and the WJ-MSC human umbilical cord mesenchymal stem cells even at the highest concentrations tested.

Journal Pre-proof

Journal Pre-proof

Conflict of Interest and Authorship Conformation Form

Please check the following as appropriate:

X All authors have participated in (a) conception and design, or analysis and interpretation of the data; (b) drafting the article or revising it critically for important intellectual content; and (c) approval of the final version.

X This manuscript has not been submitted to, nor is under review at, another journal or other publishing venue.

X The authors have no affiliation with any organization with a direct or indirect financial interest in the subject matter discussed in the manuscript

Journal Pre-proof